

Chern Number Tunable Quantum Anomalous Hall Effect in Compensated Antiferromagnets

Wenhao Liang,¹ Jiaqi An,¹ Zeyu Li,^{1,*} Yafei Ren,^{2,†} Zhenhua Qiao,^{1,3,‡} and Qian Niu¹

¹*International Centre for Quantum Design of Functional Materials, CAS Key Laboratory of Strongly-Coupled Quantum Matter Physics, and Department of Physics, University of Science and Technology of China, Hefei, Anhui 230026, China*

²*Department of Physics and Astronomy, University of Delaware, Newark, Delaware 19716, USA*

³*Hefei National Laboratory, University of Science and Technology of China, Hefei 230088, China*

(Dated: April 23, 2024)

We propose to realize quantum anomalous Hall effect (QAHE) in two-dimensional antiferromagnetic topological insulators. We consider antiferromagnetic MnBi_2Te_4 as a concrete example. In contrast to the even-layer A-type antiferromagnetic MnBi_2Te_4 that has zero Chern number due to the combined parity-time (\mathcal{PT}) symmetry, the system can host a nonzero Chern number by breaking this symmetry. We show that by controlling the antiferromagnetic spin configuration, for example, down/up/up/down, to break \mathcal{PT} symmetry, tetralayer antiferromagnetic MnBi_2Te_4 can realize QAHE with Chern number $\mathcal{C} = -1$. Such spin configuration can be stabilized by pinning the spin orientations on top and bottom layers. Furthermore, we reveal that the edge states are layer-selective and primarily locate at the boundaries of the bottom and top layers. In addition, via tuning the on-site orbital energy which determines the inverted band gap, we find tunable Chern number from $\mathcal{C} = -1$ to $\mathcal{C} = 2$ and then to $\mathcal{C} = -1$. Our work not only proposes a scheme to realize Chern number tunable QAHE in antiferromagnets without net spin magnetization, but also provide a platform for layer-selective dissipationless transport devices.

The quantum anomalous Hall effect (QAHE) exhibits topologically protected chiral edge states, the dissipationless feature of which makes them attractive for next-generation high-performance electronics [1]. The QAHE also shows close connection with novel quantum phenomena such as topological magnetoelectric effects and topological superconductivity [2–4]. The search for QAHE is thus a hot spot in condensed matter physics [5–7] with many recipes being theoretically proposed [8–22]. In experiments, the QAHE has been observed in three main categories, i.e., magnetic doped topological insulators [23], intrinsic magnetic topological insulators [24] and moiré systems [25, 26]. All of them possess ferromagnetism, which can be influenced by fluctuations of external magnetic fields that can arise from stray fields or other external sources, which is not desired in applications. In contrast, antiferromagnets are more robust to fluctuations of magnetic fields [28] and has attracted growing attention in recent years, which extended the traditional spintronics to antiferromagnetic spintronics [28–36]. The realization of QAHE in antiferromagnets is thus highly desired for applications. Despite several theoretical proposals of realizing QAHE in antiferromagnetic systems [37–47], it is still challenging to realize Chern number tunable QAHE in compensated antiferromagnets without net spin magnetization.

In this letter, we propose to realize the antiferromagnetic QAHE in an experimentally feasible system, i.e., the magnetic topological insulator system, by controlling the spin configuration. We consider the tetralayer antiferromagnetic MnBi_2Te_4 as an example. The typical A-type antiferromagnetic spin configuration (e.g.,

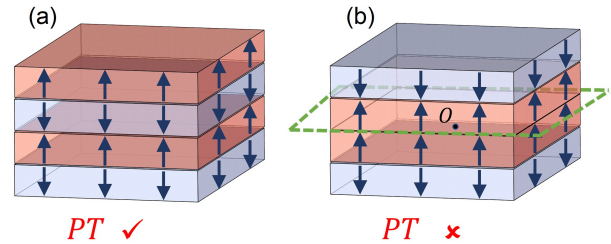


FIG. 1. The tetralayer system of an (a) intrinsic A-type antiferromagnet with \mathcal{PT} symmetry, and (b) antiferromagnet without \mathcal{PT} symmetry. The latter is composed of two bilayer antiferromagnets (separated by the green dashed line), where the upper bilayer is head-to-head, and the lower tail-to-tail. The space inversion point is denoted by O .

down/up/down/up) is invariant under \mathcal{PT} operation where \mathcal{P} is parity and \mathcal{T} is the time-reversal operation as illustrated in Fig. 1(a). This symmetry guarantees a zero Chern number. By reversing the spins of the top two layers as illustrated in Fig. 1(b), the \mathcal{PT} symmetry is broken as the system now is even under \mathcal{P} whereas is odd under \mathcal{T} . The breaking of both \mathcal{PT} and \mathcal{T} symmetries allows the presence of a nonzero Chern number. Despite the fact that the spin configuration in Fig. 1(b) is energetically less favorable than the intrinsic A-type antiferromagnetic spin configuration in Fig. 1(a), it can be realized by introducing magnetic pinning layer that fix the spin configuration of the top and bottom layers.

Structure and model. — We focus on the intrinsic magnetic topological insulator MnBi_2Te_4 [48–59], where Mn atoms form magnetic layers. The intralayer spin-spin interaction is ferromagnetic forming a ferromagnetic layer.

The neighboring layers are coupled antiferromagnetically, resulting in an A-type antiferromagnetic configuration, which is invariant under the \mathcal{PT} operation and thus ensures a zero Chern number [51]. To realize QAHE, this symmetry must be broken [53]. Here, we break this symmetry by controlling the spin configuration as shown in Fig. 1(b).

The tetralayer antiferromagnetic topological insulator system can be described by the model Hamiltonian [55–61]

$$H = \sum_i c_i^\dagger (E_0 + \nu_i m) c_i + \sum_{\langle ij \rangle, \alpha} c_i^\dagger T_\alpha c_j + \text{H.c.}, \quad (1)$$

where $c_i = \{|+\uparrow\rangle, |-\uparrow\rangle, |+\downarrow\rangle, |-\downarrow\rangle\}^T$ is the electronic state at site i , \pm represent two different orbits and (\uparrow, \downarrow) denote spin indices. $E_0 = (t_A \sigma_0 \otimes \tau_z - \frac{3}{2} A \sigma_0 \otimes \tau_0)$ and $T_\alpha = \frac{3}{2} (t_B \sigma_0 \otimes \tau_z + A \sigma_0 \otimes \tau_0 - iB \sigma_\alpha \otimes \tau_x)$ with $\alpha = x, y, z$. The Pauli matrices σ and τ are for the spin and orbit degrees of freedom, respectively. $\langle ij \rangle$ denotes the nearest neighboring coupling. $m = m_0 \sigma_z \otimes \tau_0$ is the exchange field and $\nu_i = \{-1, 1, 1, -1\}$ for different layers, representing down/up/up/down spin configuration. The parameter B reflects the Fermi velocity, and t_A is the on-site orbital energy which determines the inverted band gap. In experiments, t_A can be controlled by atomic doping and pressure. Without loss of generality, we set the parameters to be $A = 0.1, B = 1.5, m_0 = 0.35$ [60], and $t_B = 1$ as the energy unit.

Band structures and topological properties.— The spin compensated antiferromagnetic topological insulator with down/up/up/down spin configuration can host a Chern insulator phase. Figure 2 shows the band structures and Berry curvature distributions at various t_A . The band structure at $t_A = -1.5$ is plotted in Fig. 2(a) where the bands are non-degenerate since the \mathcal{PT} symmetry is broken. The valance band maximum and conduction band minimum are dominated by spin-down (blue) and spin-up (red) electrons, respectively. The band gap is topologically trivial as the positive and negative Berry curvatures (see the inset) cancel in the first Brillouin zone resulting in a vanished Chern number $\mathcal{C} = 0$. The band gap decreases with increasing t_A , and at $t_A = -1.38$, a Dirac point emerges at Γ point [see Fig. 2(b)]. When t_A exceeds -1.38 , the band gap reopens, accompanied by the switch of spin between the valance band maximum and conduction band minimum [see Fig. 2(c)]. In this case, only negative Berry curvatures emerge concentrated at the Γ point, leading to Chern number $\mathcal{C} = -1$, i.e., the system goes into the QAHE states. This topologically nontrivial phase persists until t_A is further increased to -0.62 [see Fig. 2(d)].

In terms of MnBi_2Te_4 , the parameters $t_B \simeq 47$ meV and $t_A = -t_B$ can faithfully reproduce the band gap and band topology for antiferromagnetic MnBi_2Te_4 trilayer (down/up/down) (see Supplementary Materials

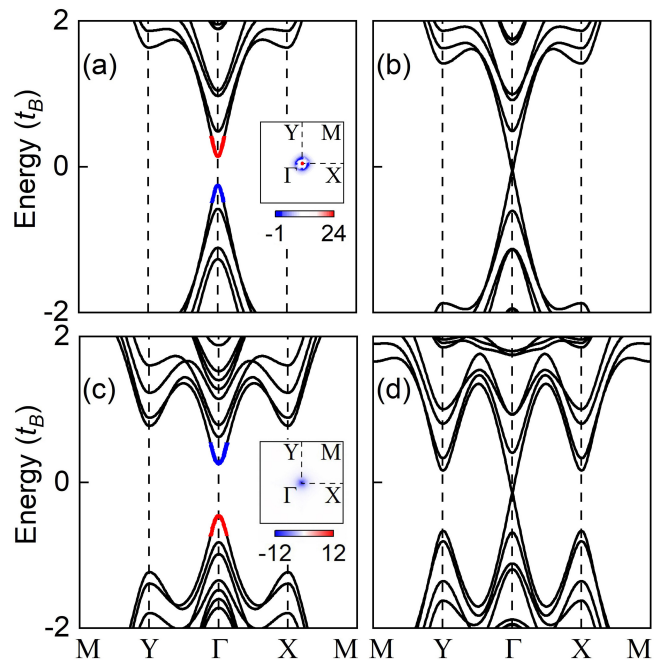


FIG. 2. Bulk band structures along the high symmetry lines of tetralayer antiferromagnetic systems without \mathcal{PT} symmetry: (a) $t_A = -1.5$, (b) $t_A = -1.38$, (c) $t_A = -1$, (d) $t_A = -0.62$. The majority of the electronic spin is up (red) or down (blue) near the Fermi level. The inset is the distribution of Berry curvatures in the momentum space, with black lines marking the first Brillouin zone.

[63]). Therefore, the nontrivial band topology at $t_A = -1$ indicates that a topologically nontrivial phase with $\mathcal{C} = -1$ can be realized in tetralayer MnBi_2Te_4 with down/up/up/down spin configuration.

Phase diagram.— We further study the topological phase diagram of this model systematically to identify the parameter space of realizing the antiferromagnetic QAHE. Keeping the increase of t_A , the band structures of even-layer antiferromagnetic system are notably deformed, as shown in Fig. 2. When $t_A = -0.5$, the valance band maximum and conduction band minimum migrate to X/Y points, with positive and negative Berry curvature distributing at Γ and X/Y points, respectively. When $t_A = -0.38$, two Dirac points are formed at X/Y points. After t_A exceeds -0.38 , the band inversion occurs again near the Fermi level, i.e., another topological phase transition emerges. As shown in Fig. 3(c), only positive Berry curvatures are observed at X and Y points. Since the Berry curvature around each X or Y point contributes 1 to the total Chern number, the system enters another QAHE state and Chern number $\mathcal{C} = 2$. With the further increase of t_A , at X and Y points, two Dirac points are formed and gaped sequentially, leading to a transition of the system into a topologically trivial phase [Fig. 3(e)]. And the positive and negative Berry curvatures distribute, respectively, at M with X/Y points.

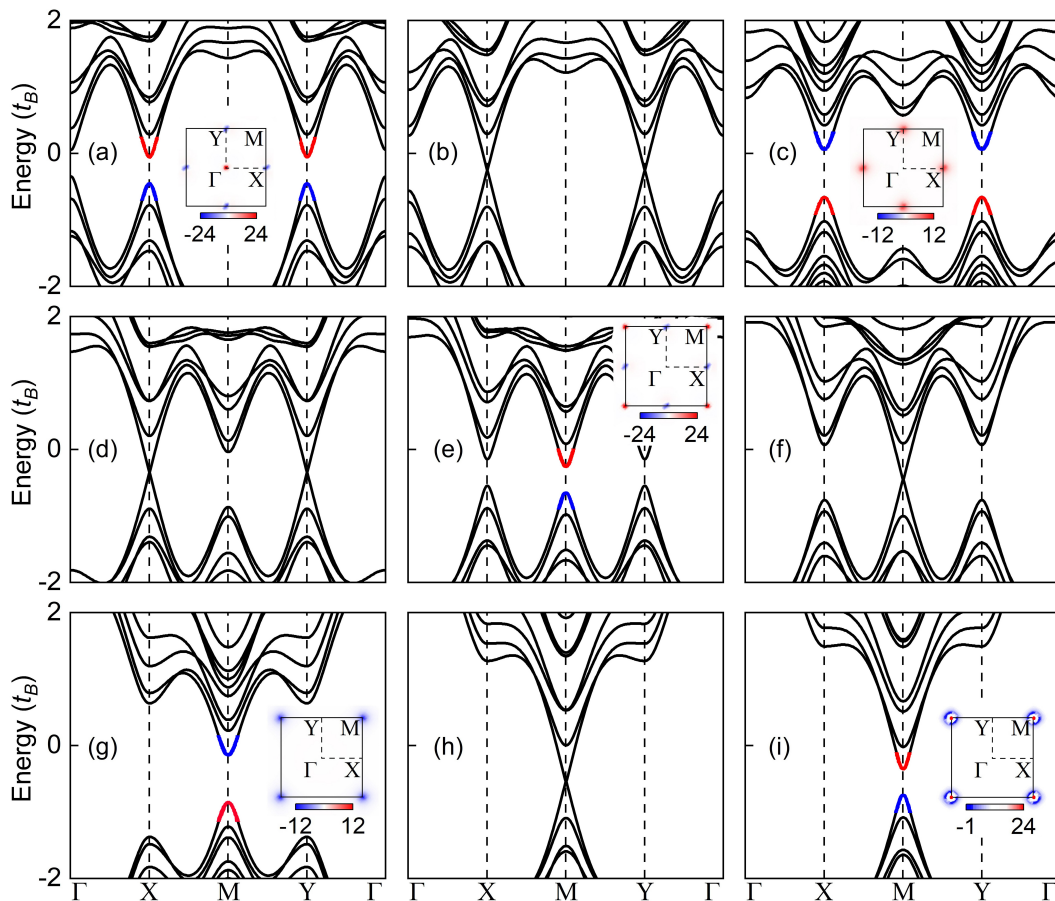


FIG. 3. Bulk band structures evolution of tetralayer antiferromagnetic systems with different t_A : (a) $t_A = -0.5$, (b) $t_A = -0.38$, (c) $t_A = 0$, (d) $t_A = 0.38$, (e) $t_A = 0.5$, (f) $t_A = 0.62$, (g) $t_A = 1$, (h) $t_A = 1.38$, and (i) $t_A = 1.5$. The majority of the electronic spin is up (red) or down (blue) near the Fermi level. The inset is the distribution of Berry curvatures in the momentum space, with black lines marking the first Brillouin zone.

When $t_A = 0.62$, the valance band maximum and conduction band minimum migrate to M point forming one Dirac point. After t_A exceeding this value, the band gap opens and accompanies band inversion near the Fermi level [see Fig. 3(g)]. Accordingly, the system possesses negative Berry curvatures concentrated at M point. This distribution of Berry curvatures reveals that it is a Chern insulator with $C = -1$. When $t_A = 1.38$, a Dirac point is formed at M point [Fig. 3(h)]. Under even stronger $|t_A|$, the system goes into a topologically trivial phase where the band gap increases monotonically.

The phase diagram is plotted in Fig. 4 where the band gap is plotted in black solid line as a function of t_A . The system undergoes band gap closing and reopening for six times. During this process, the band gap closing migrates from Γ point to X/Y points, and subsequently to M point. The migration of Dirac points induces the redistribution of Berry curvatures leading to a tunable Chern number ranging from -1 to 2 and then to -1 as indicated by color. It is noteworthy that although the system has two QAHE phases with $C = -1$ successively, they have dis-

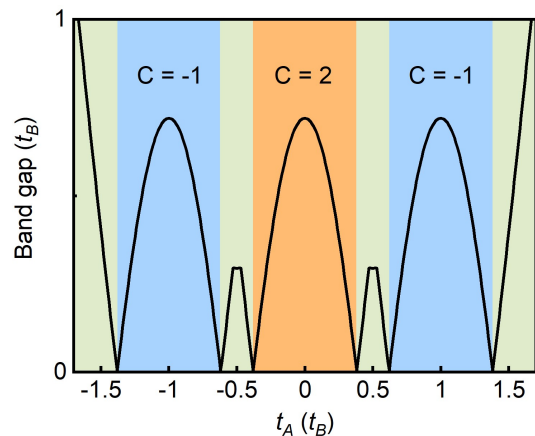


FIG. 4. The phase diagram of Chern number as a function of t_A for the tetralayer antiferromagnetic system.

tinct distributions of the Berry curvatures and different band structures.

Layer-selective edge states.— As a multi-layer sys-

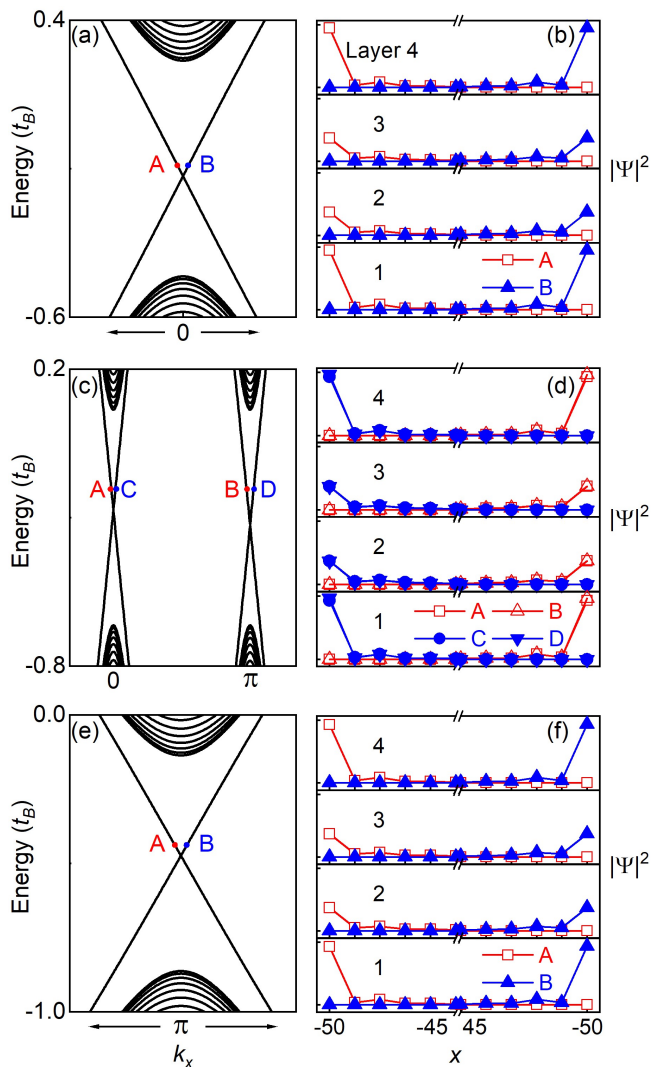


FIG. 5. The first column: the one-dimensional energy spectrum of three different topologically nontrivial phases for (a) $t_A = -1$, (c) $t_A = 0$, and (e) $t_A = 1$, where the different edge states near the charge neutral point are labeled as “A”, “B”, “C” and “D”. The second column: The corresponding wavefunction distributions $|\psi|^2$ of different edge states in each layer, with values ranging from 0 to 0.32 in each layer. A break is taken on the x -axis since the values within the break range are zero.

tem, even-layer MnBi_2Te_4 possesses the spatial degree of freedom corresponding to different layers, which will bring new features to electronic and topological properties [53, 58]. Figure 5(a) displays the one-dimensional band structure of the system of $t_A = -1$ corresponding to a Chern number $\mathcal{C} = -1$. There are a pair of gapless chiral edge states at $k_x = 0$, whose wavefunction distributions are depicted in Fig. 5(b). State A with negative velocity is located at the left boundary. It is noted that the probability density distribution of this states is not equally divided in each layer. The wavefunction distribution concentrates on top and bottom layers, which are

much larger than the probability density in the middle two layers. The distributions in top and bottom layers are the same guaranteed by the inversion symmetry. The case is similar for state B, which is the inversion counterpart of the state A localized on the opposite boundary with opposite velocity.

When $t_A = 0$, the system is a Chern insulator with Chern number $\mathcal{C} = 2$. According to bulk-boundary correspondence [62], there are two pairs of gapless chiral edge states as shown in Fig. 5(c) where two pairs of edge states appear at $k_x = 0$ and $k_x = \pi$ respectively. The modulus squared of wavefunction distribution [see Fig. 5(d)] indicate that the edge states are also mainly distributed in the bottom and top layers. Similarly, the system of $t_A = 1$ is a Chern insulator with $\mathcal{C} = -1$, and the corresponding chirality is identical to that of $t_A = -1$. Its chiral edge states at $k_x = \pi$ [see Fig. 5(e)] are also mainly distributed in the bottom and top layers, as shown in Fig. 5(f). For all three different topologically nontrivial phases, the edge states are mainly distributed at the boundaries of the bottom and top layers. Such layer-selective phenomena can be applied in layer-selective dissipationless transport devices. This behavior is also illustrated by our calculations of the local density of states [63].

Stability of the spin configuration.— Although the spin configuration in our proposal is not the lowest-energy states compared to the intrinsic A-type antiferromagnetic configuration, it can be achieved by pinning the top and the bottom magnetic layers [64], which is widely used in magnetic tunneling junctions. By including pinning layers, one can pin the spin configurations of the top and the bottom layers to be, for example, downward. Here we show that, in this case, the down/up/up/down spin configuration is the lowest energy configuration. We consider a Heisenberg spin model to describe the spin configuration that reads

$$H^s = J_c \sum_{\langle ij \rangle} \mathbf{S}_i \cdot \mathbf{S}_j - D \sum_i (\mathbf{S}_i \cdot \hat{z})^2, \quad (2)$$

where \mathbf{S}_i labels the spin at layer i

$$\mathbf{S}_i = \{\sin(\theta_i) \cos(\phi_i), \sin(\theta_i) \sin(\phi_i), \cos(\theta_i)\}, \quad (3)$$

with θ and ϕ being the spin polar and azimuthal angles, respectively. $J_c > 0$ is the interlayer magnetic exchange interaction between the nearest-neighbor layers $\langle ij \rangle$, D is the uniaxial magnetic anisotropy. The pinning effect fix the spin orientations at the top and bottom layers with $\theta_1 = \theta_4 = \pi$. The spin orientations of the middle two layers is determined by the lowest energy configuration. Given the parameters $J_c = 0.034$ meV and $D = 0.03$ meV in MnBi_2Te_4 [65], our calculation shows that the spin configuration has lowest energy at $\theta_2 = \theta_3 = 0$. Therefore, our spin configuration of down/up/up/down is stable when we pinned the top and bottom layers.

Summary.— We systematically investigate the electronic and topological properties of two-dimensional compensated antiferromagnetic systems. Taking even-layer MnBi_2Te_4 as an example, the QAHE can be realized by breaking \mathcal{PT} symmetry through the controlling of layer stacking order. And such spin magnetic configuration can be realized by pinning effect. Furthermore, the position of Dirac points and the distribution of Berry curvatures are successively tuned via tuning the on-site orbital energy which determines the inverted band gap, giving rise to Chern number tunable QAHE. We also find that the edge states are layer-selective, i.e., primarily distributed at the boundaries of the bottom and top layers. Our work not only provides an ideal platform to realize Chern number tunable QAHE and Berry curvature engineering in compensated antiferromagnets, but also sheds light on layer-selective dissipationless transport for practical applications.

Our results in the tetralayer compensated antiferromagnetic system can be generalized to multi-layer systems. We demonstrate in the Supplementary Materials [63] that the electronic and topological properties of multi-layer systems are almost identical to the tetralayer system. Furthermore, what we studied is a general model, which is not limited to MnBi_2Te_4 . Our results are generally applicable to layered antiferromagnetic topological insulator materials.

We are grateful to Prof. F. L. for his valuable discussions. W. L., J. A. and Z. Q. are supported by the National Natural Science Foundation of China (Grants No. 11974327 and No. 12004369), Natural Science Basic Research Program of Shanxi (No. 20210302124252), Anhui Initiative in Quantum Information Technologies (AHY170000), and Innovation Program for Quantum Science and Technology (2021ZD0302800). Z. L. is supported by China Postdoctoral Science Foundation (2023M733411 and 2023TQ0347). Y. R. acknowledges startup funds provided by the College of Arts and Sciences and the Department of Physics and Astronomy of the University of Delaware. Q. N. is supported by the National Natural Science Foundation of China (Grant No. 12234017). We also thank the Supercomputing Center of University of Science and Technology of China for providing the high performance computing resources.

* Correspondence author: lzy92@ustc.edu.cn

† Correspondence author: yfren@udel.edu

‡ Correspondence author: qiao@ustc.edu.cn

- [1] H. Weng, R. Yu, X. Hu, X. Dai and Z. Fang, Quantum anomalous Hall effect and related topological electronic states, *Adv. Phys.* **64**, 227-282 (2015).
- [2] K. He, Y. Wang, and Q.-K. Xue, Topological Materials: Quantum Anomalous Hall System, *Annu. Rev. Condens. Matter Phys.* **9**, 329 (2018).
- [3] D. Xiao, J. Jiang, J.-H. Shin, W. Wang, F. Wang, Y.-F. Zhao, C. Liu, W. Wu, M. H. W. Chan, N. Samarth et al., Chang, Realization of the Axion Insulator State in Quantum Anomalous Hall Sandwich Heterostructures, *Phys. Rev. Lett.* **120**, 056801 (2018).
- [4] X.-L. Qi, T. L. Hughes, and S.-C. Zhang, Chiral topological superconductor from the quantum Hall state, *Phys. Rev. B* **82**, 184516 (2010).
- [5] C.-Z. Chang, C.-X. Liu, and A. H. MacDonald, Colloquium: Quantum anomalous Hall effect, *Rev. Mod. Phys.* **95**, 011002 (1988).
- [6] X.-L. Qi and S.-C. Zhang, Topological insulators and superconductors, *Rev. Mod. Phys.* **83**, 1057 (2011).
- [7] M. Z. Hasan and C. L. Kane, Colloquium: Topological insulators, *Rev. Mod. Phys.* **82**, 3045 (2010).
- [8] C.-X. Liu, X.-L. Qi, X. Dai, Z. Fang, and S.-C. Zhang, Quantum Anomalous Hall Effect in $\text{Hg}_{1-y}\text{Mn}_y\text{Te}$ Quantum Wells, *Phys. Rev. Lett.* **101**, 146802 (2008).
- [9] R. Yu, W. Zhang, H.-J. Zhang, S.-C. Zhang, X. Dai, and Z. Fang, Quantized Anomalous Hall Effect in Magnetic Topological Insulators, *Science* **329**, 61 (2010).
- [10] Z. Qiao, S. A. Yang, W.-X. Feng, W.-K. Tse, J. Ding, Y. G. Yao, J. Wang, and Q. Niu, Quantum anomalous Hall effect in graphene from Rashba and exchange effects, *Phys. Rev. B* **82**, 161414(R) (2010).
- [11] K. F. Garrity and D. Vanderbilt, Chern Insulators from Heavy Atoms on Magnetic Substrates, *Phys. Rev. Lett.* **110**, 116802 (2013).
- [12] C. Fang, M. J. Gilbert, and B. A. Bernevig, Large-Chern-Number Quantum Anomalous Hall Effect in Thin-Film Topological Crystalline Insulators, *Phys. Rev. Lett.* **112**, 046801 (2014).
- [13] Y. Ren, J. Zeng, X. Deng, F. Yang, H. Pan, and Z. Qiao, Quantum anomalous Hall effect in atomic crystal layers from in-plane magnetization, *Phys. Rev. B* **94**, 085411 (2016).
- [14] H. P. Wang, W. Luo, and H. J. Xiang, Prediction of high-temperature quantum anomalous Hall effect in two-dimensional transition-metal oxides, *Phys. Rev. B* **95**, 125430 (2017).
- [15] M. M. Otrokov, I. P. Rusinov, M. Blanco-Rey, M. Hoffmann, A. Y. Vyazovskaya, S. V. Eremeev, A. Ernst, P. M. Echenique, A. Arnau, and E. V. Chulkov, Unique Thickness-Dependent Properties of the van der Waals Interlayer Antiferromagnet MnBi_2Te_4 Films, *Phys. Rev. Lett.* **122**, 107202 (2019).
- [16] F. Wu, T. Lovorn, E. Tutuc, I. Martin, and A. H. MacDonald, Topological Insulators in Twisted Transition Metal Dichalcogenide Homobilayers, *Phys. Rev. Lett.* **122**, 086402 (2019).
- [17] Y.-H. Zhang, D. Mao, Y. Cao, P. Jarillo-Herrero, and T. Senthil, Nearly flat Chern bands in moiré superlattices, *Phys. Rev. B* **99**, 075127 (2019).
- [18] N. Bultinck, S. Chatterjee, and M. P. Zaletel, Mechanism for Anomalous Hall Ferromagnetism in Twisted Bilayer Graphene, *Phys. Rev. Lett.* **124**, 166601 (2020).
- [19] J. Shi, J. Zhu, and A. H. MacDonald, Moiré commensurability and the quantum anomalous Hall effect in twisted bilayer graphene on hexagonal boron nitride, *Phys. Rev. Lett.* **103**, 075122 (2021).
- [20] G. Chen, A. L. Sharpe, E. J. Fox, Y.-H. Zhang, S. Wang, L. Jiang, B. Lyu, H. Li, K. Watanabe, T. Taniguchi et al., and F. Wang, Tunable correlated Chern insulator and ferromagnetism in a moiré superlattice, *Nature* **579**, 56

- (2020).
- [21] Z. Li, Y. Han, and Z. Qiao, Chern Number Tunable Quantum Anomalous Hall Effect in Monolayer Transitional Metal Oxides via Manipulating Magnetization Orientation, *Phys. Rev. Lett.* **129**, 036801 (2022).
- [22] Feng Liu, Two-dimensional topological insulators: past, present, and future, *Coshare Science*, **01**, v3, 1-62 (2023).
- [23] C. Z. Chang, J. S. Zhang, X. Feng, J. Shen, Z. C. Zhang, M. H. Guo, K. Li, Y. B. Ou, P. Wei, L. L. Wang, et al., Experimental Observation of the Quantum Anomalous Hall Effect in a Magnetic Topological Insulator, *Science* **340**, 167 (2013).
- [24] Y. Deng, Y. Yu, M. Z. Shi, Z. Guo, Z. Xu, J. Wang, X. H. Chen, and Y. Zhang, Quantum anomalous Hall effect in intrinsic magnetic topological insulator MnBi_2Te_4 , *Science* **367**, 895 (2020).
- [25] M. Serlin, C. L. Tschirhart, H. Polshyn, Y. Zhang, J. Zhu, K. Watanabe, T. Taniguchi, L. Balents, and A. F. Young, Intrinsic quantized anomalous Hall effect in a moiré heterostructure, *Science* **367**, 900 (2020).
- [26] T. Li, S. Jiang, B. Shen, Y. Zhang, L. Li, Z. Tao, T. Devakul, K. Watanabe, T. Taniguchi, L. Fu et al., Quantum anomalous Hall effect from intertwined moiré bands, *Nature* **600**, 641 (2021).
- [27] C.-X. Liu, S.-C. Zhang, and X.-L. Qi, The Quantum Anomalous Hall Effect: Theory and Experiment, *Annu. Rev. Condens. Matter Phys.* **7**, 301 (2016).
- [28] V. Baltz, A. Manchon, M. Tsoi, T. Moriyama, T. Ono, and Y. Tserkovnyak, Antiferromagnetic spintronics, *Rev. Mod. Phys.* **90**, 015005 (2018).
- [29] T. Jungwirth, X. Marti, P. Wadley, and J. Wunderlich, Antiferromagnetic spintronics, *Nat. Nanotechnol.* **11**, 231 (2016).
- [30] L. Šmejkal, Y. Mokrousov, B. Yan and A. H. MacDonald, Topological antiferromagnetic spintronics, *Nat. Phys.* **14**, 242 (2018).
- [31] P. Němec, M. Fiebig, T. Kampfrath and A. V. Kimel, Antiferromagnetic opto-spintronics, *Nat. Phys.* **14**, 229 (2018).
- [32] S. Rahman, J. F. Torres, A. R. Khan, and Y. Lu, Recent Developments in van der Waals Antiferromagnetic 2D Materials: Synthesis, Characterization, and Device Implementation, *ACS Nano* **15**, 17175 (2021).
- [33] B. Huang, G. Clark, E. Navarro-Moratalla, D. R. Klein, R. Cheng, K. L. Seyler, D. Zhong, E. Schmidgall, M. A. McGuire, D. H. Cobden et al., Layer-dependent ferromagnetism in a van der Waals crystal down to the monolayer limit, *Nature* **546**, 270 (2017).
- [34] B. Huang, G. Clark, D. R. Klein, D. MacNeill, E. Navarro-Moratalla, K. L. Seyler, N. Wilson, M. A. McGuire, D. H. Cobden, D. Xiao, et al., Electrical control of 2D magnetism in bilayer CrI_3 , *Nat. Nanotech.* **13**, 544 (2018).
- [35] W. Chen, Z. Sun, Z. Wang, L. Gu, X. Xu, S. Wu, and C. Gao, Direct observation of van der Waals stacking-dependent interlayer magnetism, *Science* **366**, 983 (2019).
- [36] Z. Sun, Y. Yi, T. Song, G. Clark, B. Huang, Y. Shan, S. Wu, D. Huang, C. Gao, Z. Chen et al., Giant nonreciprocal second-harmonic generation from antiferromagnetic bilayer CrI_3 , *Nature* **572**, 497 (2019).
- [37] P. Zhou, C. Q. Sun, and L. Z. Sun, Two Dimensional Antiferromagnetic Chern Insulator: NiRuCl_6 , *Nano. Lett.* **16**, 6325 (2016).
- [38] J. Wang, Antiferromagnetic Dirac semimetals in two dimensions, *Phys. Rev. B* **95**, 115138 (2017)
- [39] K. Jiang, S. Zhou, X. Dai, and Z. Wang, Antiferromagnetic Chern Insulators in Noncentrosymmetric Systems, *Phys. Rev. Lett.* **120**, 157205 (2018)
- [40] X. Li, A. H. MacDonald, and H. Chen, Quantum Anomalous Hall Effect through Canted Antiferromagnetism, *arXiv:1902.10650* (2019).
- [41] P.-J. Guo, Z.-X. Liu and Z.-Y. Lu, Quantum anomalous hall effect in collinear antiferromagnetism, *npj Comput. Mater.* **9**, 70 (2023)
- [42] B. Wu, Y.-L. Song, W.-X. Ji, P.-J. Wang, S.-F. Zhang, and C.-W. Zhang, Quantum anomalous Hall effect in an antiferromagnetic monolayer of MoO , *Phys. Rev. B* **107**, 214419 (2023)
- [43] M. Ebrahimkhas, G. S. Uhrig, W. Hofstetter, and M. Hafez-Torbati, Antiferromagnetic Chern insulator in centrosymmetric systems, *Phys. Rev. B* **106**, 205107 (2022)
- [44] S. Du, P. Tang, J. Li, Z. Lin, Y. Xu, W. Duan, and A. Rubio, Berry curvature engineering by gating two-dimensional antiferromagnets, *Phys. Rev. Research* **2**, 022025(R) (2020)
- [45] C. Lei, T. V. Trevisan, O. Heinonen, R. J. McQueeney, and A. H. MacDonald, Quantum anomalous Hall effect in perfectly compensated collinear antiferromagnetic thin films, *Phys. Rev. B* **106**, 195433 (2022)
- [46] X. Zhou, W. Feng, Y. Li, and Y. Yao, Spin-Chirality-Driven Quantum Anomalous and Quantum Topological Hall Effects in Chiral Magnets, *Nano Lett.* **23**, 5680-5687 (2023)
- [47] Y. Liu, J. Li and Q. Liu, Chern-Insulator Phase in Antiferromagnets, *Nano Lett.* **23**, 8650-8656 (2023)
- [48] M. M. Otrokov, I. I. Klimovskikh, H. Bentmann, D. Estyunin, A. Zeugner, Z. S. Aliev, S. Gaß, A. U. B. Wolter, A. V. Koroleva, A. M. Shikin et al., Prediction and observation of an antiferromagnetic topological insulator, *Nature* **576**, 416 (2019)
- [49] J. Li, C. Wang, Z. Zhang, B.-L. Gu, W. Duan, and Y. Xu, Magnetically controllable topological quantum phase transitions in the antiferromagnetic topological insulator MnBi_2Te_4 , *Phys. Rev. B* **100**, 121103(R) (2019)
- [50] W. Liang, J. Zeng, Z. Qiao, Y. Gao, and Q. Niu, Berry-Curvature Engineering for Nonreciprocal Directional Dichroism in Two-Dimensional Antiferromagnets, *Phys. Rev. Lett.* **131**, 256901 (2023).
- [51] J. Li, Y. Li, S. Du, Z. Wang, B. L. Gu, S. C. Zhang, K. He, W. Duan, and Y. Xu, Intrinsic magnetic topological insulators in van der Waals layered MnBi_2Te_4 -family materials, *Sci. Adv.* **5**, eaaw5685 (2019).
- [52] J. Ge, Y. Liu, J. Li, H. Li, T. Luo, Y. Wu, Y. Xu, and J. Wang, High-Chern-number and high-temperature quantum Hall effect without Landau levels, *Natl. Sci. Rev.* **7**, 1280 (2020).
- [53] A. Gao, Y.-F. Liu, C. Hu, J.-X. Qiu, C. Tzschaschel, B. Ghosh, S.-C. Ho, D. Bérubé, R. Chen, H. Sun et al., Layer Hall effect in a 2D topological axion antiferromagnet, *Nature* **595**, 521 (2021).
- [54] P. M. Sass, W. Ge, J. Yan, D. Obeysekera, J. J. Yang, and W. Wu, Magnetic Imaging of Domain Walls in the Antiferromagnetic Topological Insulator MnBi_2Te_4 , *Nano Lett.* **20**, 2609-2614 (2020).
- [55] D. Zhang, M. Shi, T. Zhu, D. Xing, H. Zhang, and J. Wang, Topological Axion States in the Magnetic Insulator MnBi_2Te_4 with the Quantized Magnetoelectric Ef-

- fect, Phys. Rev. Lett. **122**, 206401 (2019).
- [56] H. Sun, B. Xia, Z. Chen, Y. Zhang, P. Liu, Q. Yao, H. Tang, Y. Zhao, H. Xu, and Q. Liu, Rational Design Principles of the Quantum Anomalous Hall Effect in Superlattice-like Magnetic Topological Insulators, Phys. Rev. Lett. **123**, 096401 (2019).
- [57] H.-P. Sun, C. M. Wang, S.-B. Zhang, R. Chen, Y. Zhao, C. Liu, Q. Liu, C. Chen, H.-Z. Lu, and X. C. Xie, Analytical solution for the surface states of the antiferromagnetic topological insulator MnBi_2Te_4 , Phys. Rev. B **102**, 241406(R) (2020).
- [58] W. Liang, T. Hou, J. Zeng, Z. Liu, Y. Han, and Z. Qiao, Layer-dependent zero-line modes in antiferromagnetic topological insulators, Phys. Rev. B **107**, 075303 (2023).
- [59] B. Lian, Z. Liu, Y. Zhang, and J. Wang, Flat Chern Band from Twisted Bilayer MnBi_2Te_4 , Phys. Rev. Lett. **124**, 126402 (2020).
- [60] H. Jiang, Z. Qiao, H. Liu, and Q. Niu, Quantum anomalous Hall effect with tunable Chern number in magnetic topological insulator film, Phys. Rev. B **85**, 045445 (2012).
- [61] H. Zhang, C.-X. Liu, X.-L. Qi, X. Dai, Z. Fang, and S.-C. Zhang, Topological insulators in Bi_2Se_3 , Bi_2Te_3 and Sb_2Te_3 with a single Dirac cone on the surface, Nat. Phys. **5**, 438 (2009).
- [62] R. S. K. Mong and V. Shivamoggi, Edge states and the bulk-boundary correspondence in Dirac Hamiltonians, Phys. Rev. B **83**, 125109 (2011)
- [63] See Supplemental Materials, which includes Ref. [15, 66].
- [64] E. Liu, Y.-C. Wu, S. Couet, S. Mertens, S. Rao, W. Kim, K. Garello, D. Crotti, S. Van Elshocht, J. De Boeck, G. S. Kar, and J. Swerts, Synthetic-Ferromagnet Pinning Layers Enabling Top-Pinned Magnetic Tunnel Junctions for High-Density Embedded Magnetic Random-Access Memory, Phys. Rev. Appl. **10**, 054054 (2018)
- [65] Y. Lai, L. Ke, J. Yan, R. D. McDonald, and R. J. McQueeney, Defect-driven ferrimagnetism and hidden magnetization in MnBi_2Te_4 , Phys. Rev. B **103**, 184429 (2021)
- [66] S. Datta, Electronic Transport in Mesoscopic Systems (Cambridge University Press, Cambridge, 1997).